Free vibration analysis of variable angle-tow composite wing structures

Free vibration analysis of variable angle-tow composite wing structures

A. Viglietti[1], E. Zappino[1,*], E. Carrera[1]

[1] *MUL[2] Group, Department of Mechanical and Aerospace Engineering, Politecnico di Torino Corso Duca degli Abruzzi 24, 10129 Torino, Italy.*

Abstract

This paper investigates the possibility to improve the dynamic response of complex aeronautical structures using variable angle-tow composites. The study has been performed using an innovative numerical approach developed in the framework of the Carrera Unified Formulation able to study laminates with curvilinear fibres whose trajectories can be arbitrarily defined. Refined kinematic structural models have been used to deal with the complex behavior of such structures. Several cases have been investigated in order to validate this approach and the results have been compared with those from classical modeling approaches. Simple beam models and complex wing structures, have been considered. The effects of different fibres-paths have also been studied and compared. The results confirm that an appropriate tow lay-up can be used to improve the performances of wing structures, i.e. innovative design solutions can be achieved.

Keywords: Carrera Unified Formulation, Variable angle-tow, Beam model, Refined Model,

1. Introduction

The development of laminates characterized by curvilinear fibres can bring several advantages in order to improve the performances of composite struc-

*Corresponding author. Tel: +39 011 090 6887, e-mail: enrico.zappino@polito.it

tures. These composites, named Variable angle-tow (VAT), can be of great interest in the aerospace field because they can lead to the manufacturing of Variable Stiffness Composite laminates (VSCL) with no discontinuities inside the material maximizing the stiffness/mass ratio. In fact, as confirmed by the following results, the use of specific lamination angles can improve the structural performances such as the bending or the torsional stiffness with the risk of unexpected reduction of the other properties, e.g., unidirectional composites are suitable to increase the bending stiffness while angle-play lamination are most suitable to withstand torsional loads. The use of complex stacking sequences leads to good overall performances but reduces the effectiveness of the material orthotropy. A compromise can be found using different laminations in different areas of the structure but such approach leads to criticalities due to the presence of discontinuities inside the laminate. The use of VAT laminates can lead to an enhanced composite design. The continuous variation of the lamination angle prevents discontinuities in the structure and make it possible change the stiffness of the structure in according with the loads they have to withstand. The concept of VAT composites was proposed several years ago, and different works have been presented about this topic such as the paper by Hayer and Lee [1] where curvilinear fibres have been used to influence the stress concentration around a hole. Thanks to the development of advanced manufacturing processes such as the additive manufacturing or the automatic fibre placement the VAT materials have become more attractive for advanced structural applications and have been the topic of many theoretical studies presented in the last years.

Tornabene *et al.* [2] and Demasi *et al.* [3] evaluated displacement, strain and stress distributions of VAT plates using different refined theories. Ribeiro and Akhavan [4, 5] evaluated the linear and non-linear vibration of thin and thick VAT plates using the First-Order Shear Deformation Theory and the Third Order Shear Deformation Theory. Ribeiro [6] proposed a complete review of the mechanical behavior of VSCL panels characterized by curvilinear fibres considering the works present in the literature. The same author has presented two works about a Layer-Wise (LW) theory and a p-version finite element method

used to perform linear vibration analysis and geometrically non-linear static analyses of thin and thick variable stiffness plates [7, 8]. The large number of design variables in VAT laminates has required the use of efficient optimization techniques to obtain lamination with the desired properties. Ghiasi *et al.* [9] compared different optimization algorithms for the design of variable stiffness composite laminates. The work by Mazen *et al.* [9] offers a review of the state of the art of the optimization techniques applied in this field. Montemurro and Catapano [10] propose the use of B-spline surfaces to address the optimization problem of VAT laminate. The importance of the manufacturing constraints on the optimum design has been pointed out by the same authors [11] and the effects of the fiber steering constrains has been investigated by Peeters *et al.* [12] and Demir *et al.* [13]. One of the main problems investigated in the framework of the VSCL concerns the buckling and post-buckling behavior. Weaver and its collaborators [14, 15, 16] have studied these topics in deep extending the analyses also at the optimization of VAT composite plates [17]. Lopes *et al.* [18] have shown how the curvilinear fibres can redirect the load fluxes from a central region to a stiffer area in order to improve the buckling stiffness. More recently the post-buckling of stiffened panels with curvilinear fibres has been investigated using a Rayleigh-Ritz approach by Oliveri and Milazzo [19]. This kind of composites can also be exploited for the design of the aeroelastic response as shown in the work of [20] and its optimization [21]. The aeroelastic application has also been investigated by Standford *et al.*[22, 23] for plates and aircraft wing. In the present work, a new approach based on one-dimensional models derived from the Carrera Unified Formulation (CUF) has been used to investigate the impact of the use of Variable angle-tow composites on complex structures such as composite wing box. Essentially, the CUF allows whatever refined kinematics to be implemented quickly and easily with no need of an *ad hoc* definition of the FE matrices. This formulation has been introduced for the analysis of plate and shell by Carrera [24]. Afterward, the formulation has been extended for the beams case where the behavior of the cross-section is described with an expansion function with an arbitrary order [25]. This approach has

been widely used in literature, an example is the work by Fazzolari [26] where the free-vibration response of functionally graded beams has been investigated. In the last years, several expansions have been implemented in order to develop refined models able to provide a 3D displacement field and different levels of accuracy. In this work two main models have been used: the first one uses the Taylor-like expansions (TE Model) [25] while the second one [27] implements the Lagrange polynomials (LE Model) to describe the cross-section behavior. When LE models are considered, the unknowns are only displacements; this feature allows different structures, described by different beam formulations, to be easily joined to achieve a more complex structure. Several examples are presented in the works by Zappino *et al.* [28, 29]. The analysis of VAT laminates through refined one-dimensional models has been recently presented by Viglietti *et al.* [30]. This work proposes to exploit the capabilities of the present refined one-dimensional model to deal with complex structures [31] and its accuracy in the analysis of VAT laminate [30], to investigate the effects of the use of VAT stacks to improve the performances of multi-component structures. The present work is divided into four main parts. After this introduction, the CUF and its extension to the Variable angle-tow composites are described in short. The capabilities of the present formulation are thus demonstrated by the analysis of a rectangular thin-walled box, used for assessment and convergence analysis, and a real wing structure with a NACA profile. The last section is devoted to conclusions and remarks.

2. One-dimensional models based on the CUF

2.1. Preliminaries

Consider an arbitrary structure; the displacement vector field reads:

$$\boldsymbol{u}(x, y, z) = \{u_x \, u_y \, u_z\}^T, \tag{1}$$

The strain vector field, $\boldsymbol{\epsilon}$, is composed of six components (according to the Voigt's notation) and, considering the assumption of small displacements and

small strains, can be expressed by using the differential operator b, as [32]:

$$\boldsymbol{\epsilon} = \boldsymbol{b}\boldsymbol{u}, \tag{2}$$

The stress vector, $\boldsymbol{\sigma}$, can be retrieved from the constitutive law as

$$\boldsymbol{\sigma} = \boldsymbol{C}\boldsymbol{\epsilon}, \tag{3}$$

$\boldsymbol{C}$ is the elastic stiffness tensor that, for an orthotropic material, is characterised by nine independent elastic constants:

$$\boldsymbol{C} = \begin{bmatrix} C_{11} & C_{12} & C_{13} & 0 & 0 & 0 \\ C_{21} & C_{22} & C_{23} & 0 & 0 & 0 \\ C_{31} & C_{32} & C_{33} & 0 & 0 & 0 \\ 0 & 0 & 0 & C_{44} & 0 & 0 \\ 0 & 0 & 0 & 0 & C_{55} & 0 \\ 0 & 0 & 0 & 0 & 0 & C_{66} \end{bmatrix}. \tag{4}$$

For a multilayer plate, the stiffness tensor is defined in the material frame of each ply 1; its expression in the global frame of the laminate can be obtained by applying a standard affine transformation (i.e. a rotation) as discussed in [33]. Of course, the laminate stiffness depends upon the stacking sequence parameters, i.e. number of laminae as well as their orientations and positions within the stack.

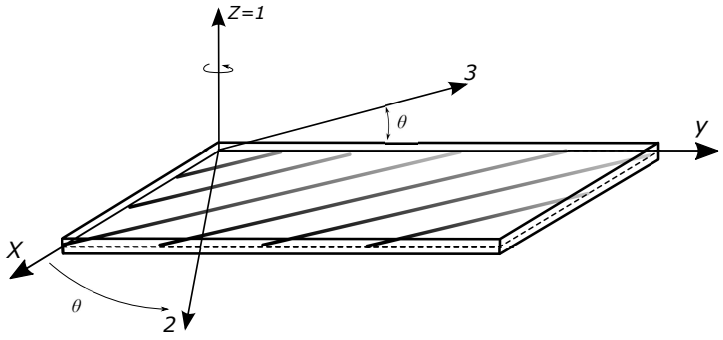

Figure 1: Material reference system

2.2. Kinematic assumption and FE solution

In the framework of the one-dimensional Carrera Unified Formulation, the displacement field of a structure, solved using the Finite Element (FE) method, is composed of two contributions. The first one is related to the kinematics used to describe the behavior of the cross-section. The second one is the axis contribution provided by the beam elements. A three-dimensional displacement field can be written as:

$$\mathbf{u}(x,y,z) = F_\tau(x,z)N_i(y)\mathbf{q}_{\tau i} \qquad \tau = 1,2\ldots M, \qquad i = 1,2\ldots N, \tag{5}$$

The cross-section kinematics can be arbitrarily chosen. Considering a single beam element, M is the number of expansion terms while N is the number of shape functions. $\mathbf{q}_{\tau i}$ is the nodal unknowns vector. The elements used in the present paper are based on the Taylor and Lagrange expansions, denoted as TE and LE respectively. The TE model, see [34] , allows the accuracy to be improved quickly by increasing the order of the expansion and it employs an Equivalent Single Layer (ESL) approach. The LE model, see [27, 31], has only displacements as degrees of freedom and allows complex geometries to be easily investigated by means of the component-wise approach described in the following sections.

The CUF provides a unified approach in the derivation of the matrices. Using the Principle of Virtual Displacement 6, the stiffness matrix can be expressed in terms of a generic 3×3 stiffness *fundamental nucleus* $\mathbf{k}^{ij\tau s}$.

$$\delta L_{int} = -\delta L_{ine}, \tag{6}$$

$$\delta L_{int} = \int_V \delta\boldsymbol{\epsilon}^T \boldsymbol{\sigma} dV, \tag{7}$$

$\boldsymbol{\sigma}$ is the stress vector and $\delta\boldsymbol{\epsilon}$ is the virtual variation of the strain defined as:

$$\delta\boldsymbol{\epsilon} = \boldsymbol{b}\delta\boldsymbol{u} = \boldsymbol{b}F_s(x,z)N_j(y)\delta\mathbf{q}_{sj}; \tag{8}$$

The internal work can be so written in the following form:

$$\delta L_{int} = \delta\mathbf{q}_{sj}^T \int_V N_j(y)F_s(x,z)\mathbf{b}^T\mathbf{C}\mathbf{b}F_\tau(x,z)N_i(y)dV\mathbf{q}_{\tau i} = \delta\mathbf{q}_{sj}^T\mathbf{k}^{ij\tau s}\mathbf{q}_{\tau i}, \tag{9}$$

where $\mathbf{k}^{ij\tau s}$ is the fundamental nucleus of the stiffness matrix. The extended form of the fundamental nucleus is reported in AppendixA. The terms of the fundamental nucleus have the same formulation for any basis of functions used to describe both cross-section kinematics and displacement interpolation along beam axis. The stiffness matrix of the element can be quickly achieved using four cycles on the indexes i, j, τ and s. The global stiffness matrix is obtained by a fifth cycle on the elements.

The same approach considering the work done by the inertial forces provides the fundamental nucleus of the Mass matrix. Information and more details about the definition of the stiffness and mass matrix can be found in the book by Carrera *et al.* [32]. The inertial work is written as:

$$\delta L_{ine} = \int_V \delta \boldsymbol{u}^T \rho \ddot{\boldsymbol{u}} dV \tag{10}$$

where ρ is the material density and $\ddot{\boldsymbol{u}}$ is the acceleration vector.

2.3. VAT models for multi-component layered structures

The analysis of complex structures requires to describe each structural component with an appropriate kinematic.Moreover, if these components are built in composite materials an high-fidelity description of the laminate is mandatory. The present model can provide an accurate description at the laminate level thanks to a layer-wise formulations and can deal with complex structures through the component-wise approach.

The Layer-wise capabilities ensured by the LE models offer an independent kinematic description for each layer of the laminate. In the case of composite materials, the results obtained by means of LW models are much more accurate that those obtained with equivalent single layer models where a unique expansion is used for all the layers. A proper cross-sectional description can be used to define the layers of the laminate. Different materials and orientation angles can be set for each layer, as shown in Figure 2. When a complex structure, characterized by several components, is investigated, each of those component can be considered as a separated entity with different proprieties, different mesh

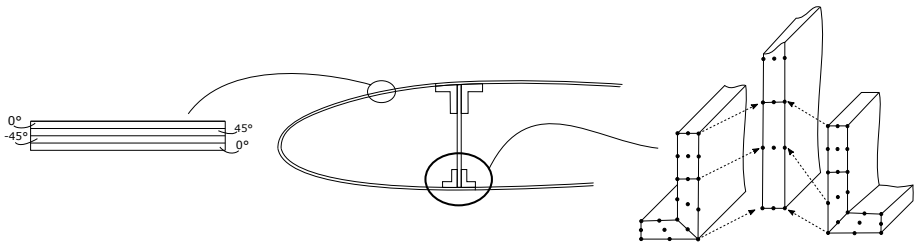

Figure 2: Layer-wise and Composite-wise approaches.

description and different kinematics, according to the requirements of the analysis. The correct assembly of the different components is guaranteed by the LE formulation where only displacements appear as unknown at each node, that is, the displacements equivalence can be easily imposed. More details about the modeling of complex structures can be found in the work by Zappino *et al.*[29].

The high-fidelity description of the multi-component structures, as well as, the refined kinematic used at the layers level, make the present approach suitable for the analysis of innovative material such as the VAT laminate.

When a VAT model is considered the fibres orientation angle, Θ, becomes a spatial variable, that is, the matrix $\boldsymbol{C}$ is no longer constant in each ply but it is function of the coordinates of the point in which is evaluated.

$$\boldsymbol{C} \longrightarrow \boldsymbol{C}(x_G, y_G, z_G). \tag{11}$$

The extension of the present one-dimensional model to the analysis of VAT laminates has been present in [30]. The new formulation requires the material properties to be included in the volume integration when the stiffness matrix terms are calculated. In the general case in which the lamination angle has a three-dimensional variation law, the integrals cannot be split into a cross-sectional and an axial contribution, as usual for the one-dimensional elements, i.e. a three-dimensional integration strategy has to be implemented.

3. Numerical Results

The results related to two different thin-walled structures are presented in this section. At first, a simple rectangular wing-box has been considered to perform the assessment and a convergence analyses of the present model. The second structure is a complete wing box with a NACA profile characterized by spars and ribs.

3.1. Thin-walled composite box

The first application concerns the analysis of a clamped prismatic box characterized by a thin-walled rectangular cross-section shown in Figure 3. A single layer box has been used for assessment purposes using a model developed by means of NX Nastran as a comparison. Then, the behavior of the same box, made by a two-layer laminate, has been investigated in order to evaluate the advantages coming from the use of VAT composites in the skin. The layers of the laminate are made of an orthotropic material with the following proprieties expressed in function of the direction of the fibre: $E_{LL} = 50\ GPa$, $E_{TT} = E_{ZZ} = 10\ GPa$, and $G_{LT} = G_{LZ} = G_{TZ} = 5\ GPa$. The Poisson's coefficients $\nu_{LT} = \nu_{LZ} = \nu_{TZ} = 0.25$. The length of the box, L, is equal to 2 m. The dimensions of the cross-section are: $a = 0.3\ m$ and $h = 0.13\ m$. Both the box and the rib have a total thickness of 0.01 m.

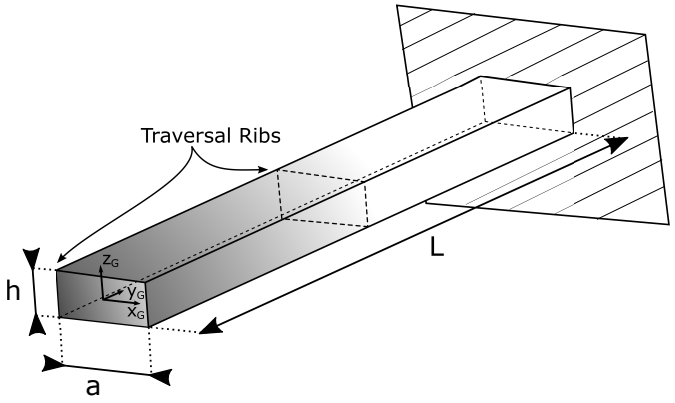

Figure 3: Geometry of the thin-walled composite box.

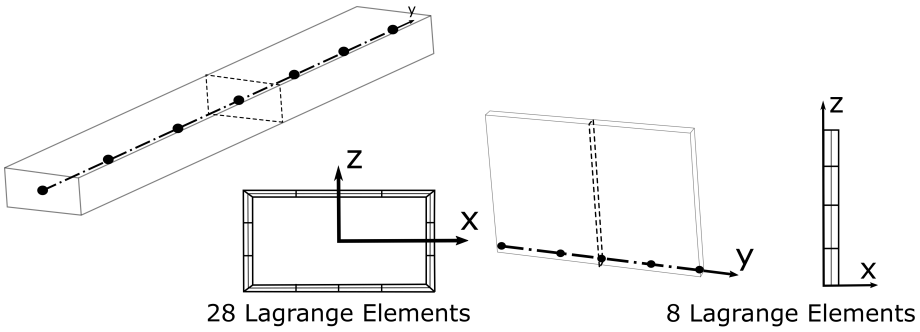

(a) FEM modeling of the box (b) FEM modeling of the rib

Figure 4: Fem description of the thin-walled box.

Figure 4 shows the modeling approach used for the structure by using the LE model. The box is described using 6 B3 beam elements and the LE description reported in Figure 4*a*. The rib is modeled through 4 B3 elements using a different beam axis orientation, as shown in 4*b*, which presents the cross-section description too.

3.1.1. Model assessment

The performances of the present approach have been assessed using a refined model, built using NX Nastran, as the reference solution. The reference model has been obtained using a spline to approximate the fibres-paths. The spline has been used to align the element reference system, that is used to define the orientation angle, with the desired direction. Using this approach a step-wise model can be obtained where each element has a different lamination angle due to the different orientations of the reference systems.

The use of this modeling technique may lead to an acceptable approximation but a proper mesh refinement has to be defined according to the complexity of the fibres-paths. For this assessment, the lamination law reported in Table 4 and denoted as case 1 is used in each panel. Models with a different refinement level have been considered in order to study the convergence of the step-wise approach. Table 1 shows the values obtained from a convergence analysis using the commercial software NX Nastran.

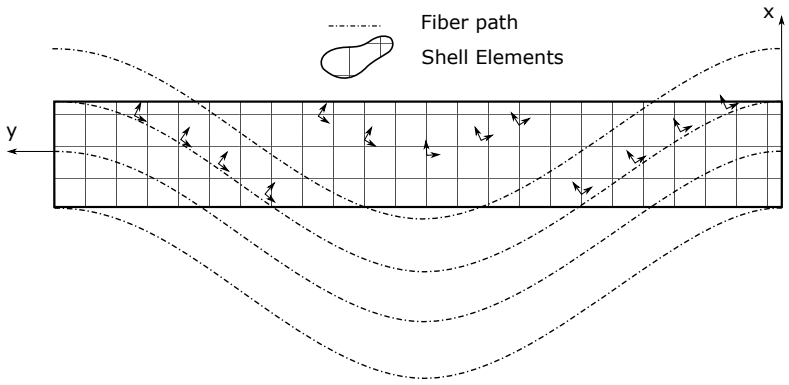

Figure 5: Description of step-wise models build up using a commercial code.

	NX Nastran			
DOFs	31710	127710	511830	1027910
1	24.52	24.33	24.22	24.13
2	48.11	47.75	47.55	47.41
3	136.67	135.59	134.98	134.39
4	164.18	164.06	163.88	163.64
5	243.47	242.01	241.19	239.44
6	257.99	257.91	257.78	255.68
7	262.56	261.79	261.40	259.57
8	263.98	262.48	261.58	260.34
9	286.58	285.46	284.72	283.00
10	322.70	321.20	320.17	316.89

Table 1: First ten natural frequencies of the single layer thin-walled box: convergence analysis using the commercial code NX Nastran.

	NX Nastran	VAT 28L9 Model				VAT 40L9 Model			
		6B3	12B3	24B3	48B3	6B3	12B3	24B3	48B3
DOFs	1027910	6666	11706	21786	41946	9068	14961	30678	59478
Mode									
1	24.13	24.23	24.07	24.05	24.04	24.19	24.03	24.01	24.01
2	47.41	47.3	46.98	46.95	46.94	47.22	46.91	46.87	46.86
3	134.39	143.74	141.07	140.57	140.47	142.94	140.23	139.7	139.57
4	163.64	169.54	168.46	168.24	168.18	167.62	166.45	166.13	165.96
5	239.44	266.72	261.36	260.53	260.38	262.69	257.35	256.45	256.27
6	255.68	297.23	296.51	295.86	295.72	286.05	285.28	284.2	284.45
7	259.57	/*	311.81	308.88	308.36	/*	299.76	296.87	296.81
8	260.34	277.23	273.44	272.77	272.64	272.87	269.29	268.66	268.51
9	283.00	307.66	304.83	303.6	303.37	296.45	293.32	292.08	291.81
10	316.89	/*	355.92	349.77	348.55	/*	344.88	338.36	337.03

/* = modal shape not detected.

Table 2: First ten natural frequencies [Hz] of the single-layer thin-walled box using different models.

The last model, that has the highest number of degrees of freedom, is used as a reference result. Table 2 reports the results achieved using two different Lagrange models and with different numbers of beam elements along the box length. The first one uses 28 quadratic elements (L9) to describe the cross-section while the second model uses a more refined kinematic with 40 L9 elements. Models with 6, 12, 24 and 48 three-node beam elements (B3) have been considered. The results provided by the current model have a good correlation with those resulting from the commercial code. Six beam elements are not enough to detect correctly the higher modes characterized by complex modal shapes. A good accuracy even for higher frequencies can be achieved with 24 beam elements and, using a refined kinematic model (L9). The more significant errors are related to modes 6 and 7 that are pure shell-like modes.

The graphs in Figure 6*a* and *b* show the convergence of the first two frequencies. The use of refined kinematic models able to take into account the variation of the orientation angle within the element, like those proposed in the present

paper, leads to a faster convergence, i.e. a lower number of degrees of freedom is required to obtain the same accuracy of the reference model.

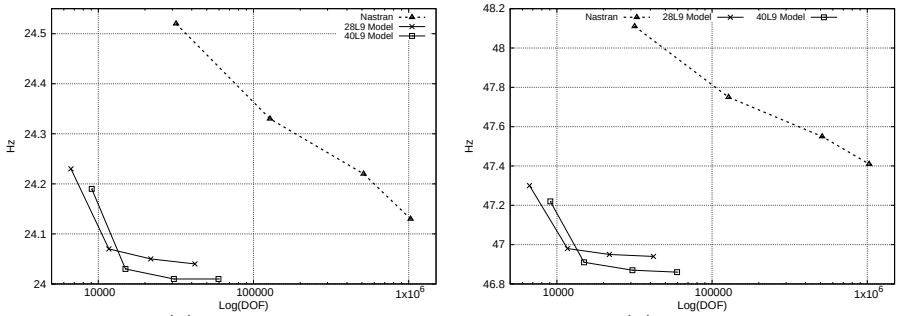

(a) Mode 1 (b) Mode 2

Figure 6: Convergence analysis of the single-layer composite box.

Figures $7a-c$ compare the modal shapes obtained using three of the present models with those evaluated using the reference solution. Figure $7a$ shows that the models built with 28L9 cross-sectional elements and 12b3 elements along the axis is able to predict the first modal shapes but is not accurate when higher frequencies are considered, see modes 10 and 11, where a large cross-sectional deformation appears. Figure $7b$ considers a model with 24b3 elements along the beam, in this case a good correlation has also been obtained for higher frequency modes. A model with a more refined cross-sectional mesh has been considered in $7c$, the use of 40L9 cross-sectional ensure a high correlation lever for each modal shape even if some modal shifts are still present.

3.1.2. Two-layer thin-walled box

The second box considered has the same geometry of the previous one but it is made by a two-layer laminate. At first, the box is investigated considering a classical lamination in order to validate the numerical model and to show the behaviors achieved by the lamination with straight fibres. Six quadratic beam elements have been used along the beam axis. Table 3 reports the results considering a unidirectional, the $90°/0°$ and the $-45°/45°$ laminations. The ribs are made by a $-45°/45°$ laminate. A layer-wise model, LE, as well as

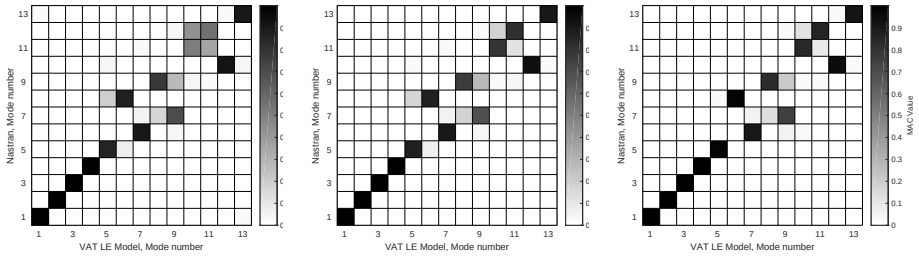

(a) VAT 28L9 with 12b3 (b) VAT 28L9 with 24b3 (c) VAT 40L9 with 48b3

Figure 7: Modal Assurance Criterion of the single-layer thin walled box between the reference model with 511830 DOFs and different VAT LE Models.

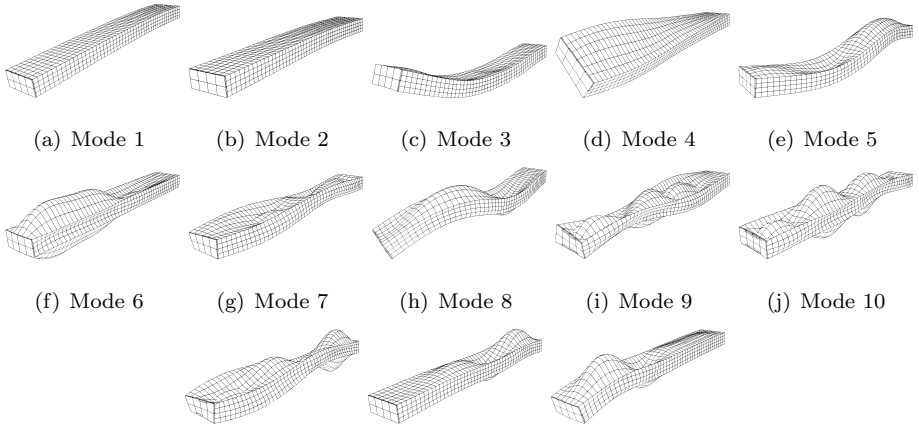

(a) Mode 1 (b) Mode 2 (c) Mode 3 (d) Mode 4 (e) Mode 5

(f) Mode 6 (g) Mode 7 (h) Mode 8 (i) Mode 9 (j) Mode 10

(k) Mode 11 (l) Mode 12 (m) Mode 13

Figure 8: Modal shapes of the single-layer thin walled box.

equivalent-single-layer models based on the Taylor expansion with a different order, TE-N, have been considered. The results obtained using a Timoshenko beam theory, TBT, have also been reported.

As expected, the unidirectional box provides the highest bending frequencies followed by the values achieved with the $90°/0°$ structure. The box has a higher torsional frequency with a $-45°/45°$ lamination the produce an increase of the 50% with respect to the unidirectional case. On the other hand, the angle-ply lamination, reduces the first bending frequencies in the two directions of about 40%, and also has a softening effect on the others bending frequencies.

The frequencies achieved from the LE model can be considered accurate if compared with the values provided by the Nastran model. The classical Timoshenko theory can predict the first bending frequencies but, as expected, the torsional model is not detected. Considering the TE models, a 4^{th} order model or higher is suggested to achieve a reasonable accuracy also for the value of the first torsional frequency.

The use of VAT composites can lead to an optimized lamination that allows a certain frequency to be maximized without a drop in the value of other frequency, as in the previous case. Table 4 reports the six trigonometric functions laws here considered for both, the panels and the webs. The coordinates x, y and z are expressed in the global reference system. An angle-ply fibres-path has been considered for both skin and webs, i.e., $\theta_p/-\theta_p$ and $\theta_w/-\theta_w$, respectively.

Figure 9 shows the fibres-paths for each law reported in Table 4. The fibre angle varies between $0°$ and $45°$. An angle equal to $0°$ has always been used at the root of the box in order to increase the bending stiffness. The fifth case introduces the lamination law in function of x and z, and it leads to a fibre overlap at the corner of the box that can be an issue in the manufacturing process. The sixth case has not been depicted since it is a combination of the fifth and fourth cases. The fibres-paths considered do not include the constraints related to the manufacturing process since the present work aims to demonstrate the capabilities of the numerical approach ant its application to to large multi-component structures. Since the present model allows an arbitrary fiber setups

	DOFs	$1-B_{xz}$	$1-B_{xy}$	$2-B_{xz}$	$1-T$	$2-B_{xy}$	$3-B_{xz}$	$2-T$	$3-T$
					$0°/0°$				
Ref.	31710	35.92	69.69	154.35	149.02	304.95	237.56	336.5	436.26
LE	6666	36.12	69.72	163.22	153.06	308.99	272.27	361.36	467.92
TBT	189	38.28	71.44	216.49	/*	339.16	552.28	/*	/*
TE1	189	38.28	71.44	216.49	210.17	339.16	552.28	1053.21	1479.25
TE2	378	38.35	71.55	216.84	175.6	339.43	552.81	531.7	906.1
TE4	945	36.97	70.8	182.7	161.26	316.9	423.56	484.85	814.49
TE8	2835	36.34	69.78	169.5	154.58	310.43	334.2	388.65	565.26
TE10	4158	36.22	69.75	166.37	152.73	309.82	303.26	354.59	454.9
					$90°/0°$				
Ref.		29.48	56.28	142.01	148.90	269.72	268.94	339.19	446.46
LE		29.84	57.03	148.26	153.07	274.98	295.33	367.73	481.78
TBT		30.83	57.73	179.48	/*	293.74	472.48	/*	/*
TE1		30.83	57.73	179.48	210.17	293.74	472.48	630.37	1053.21
TE2		31.01	58.14	180.41	174.59	295.21	474.46	527.08	893.7
TE4		30.29	57.27	160.52	160.59	278.99	388.72	803.94	1128.3
TE8		29.95	57.07	151.52	154.49	275.83	327.98	396.23	519.36
TE10		29.89	57.06	149.81	152.92	275.5	312.74	367.06	477.38
					$45°/45°$				
Ref.		21.62	41.776	124.77	219.18	238	260.93	308.8	438.28
LE		21.82	42.26	128.38	229.19	242.22	287.18	341.98	484.34
TBT		21.47	41.45	129.66	/*	234.64	357.68	/*	/*
TE1		21.47	41.45	129.66	258.6	234.64	357.68	775.6	1295.73
TE2		22.35	43.45	135.82	267.22	249.79	378.5	799.34	1330.3
TE4		22.08	42.81	132.73	259.04	245.63	363.43	756.53	1190.26
TE8		21.88	42.38	129.74	239.23	242.66	320.81	395.94	531.85
TE10		21.85	42.35	129.02	229.86	242.41	305.2	345.53	480.57

/* = modal shape not detected.

Table 3: Natural frequencies [Hz] of the two-layer thin walled box considering different modeling approaches and classical laminations.

Case #	Panles, θ_p	Webs, θ_w
Case 1	$\pi/4sin(\pi y)$	$\pi/4sin(\pi y)$
Case 2	$\pi/4sin(\pi y^2)$	$\pi/4sin(\pi y^2)$
Case 3	$\pi/4sin(y^2)$	$\pi/4sin(y^2)$
Case 4	$\pi/8(1-cos(\pi y))$	$\pi/8(1-cos(\pi y))$
Case 5	$\pi/8(1+cos(6.667\pi x))$	$\pi/8(1+cos(15.386\pi z))$
Case 6	$\pi/8(1+cos(6.667\pi y))$	$\pi/8(1-cos(\pi y))$

Table 4: Lamination laws for the six VAT configurations.

to be considered, realistic fibres-paths could be considered once defined the details of the manufacturing process, i.e. the effects of the tow curvature radius, tow width, tows gap and overlap could be taken into account.

Table 5 reports the values achieved from the analyses using the present VAT model. The results obtained from the classical theory and a 4^{th} order TE model are reported for comparison purposes.

The variation of each natural frequency, considering the different lamination schemes, is reported in Figure 10. The $x-$axis reports the lamination cases while, on the $y-$axis are reported the frequency expressed in Hz. In order to have a better understanding of the results, each mode has been depicted in a different block. Classical laminations are represented using dashed lines while the continuous line shows The VAT cases. The third $xz-$bending mode and the second $xy-$bending mode have been reported in the same block to show the frequency shift due to the lamination set-up.

The histograms reported in figure 11 are used to show the advantages of the VAT laminations considering the first four modes considering when Case 1 and Case 5 are used. Figure 11a and Figure 11d report the first bending mode and the first torsional one. As it was expected, when classical laminations are used, the unidirectional $(0/0)$ lamination produces the highest bending mode while the cross-ply lamination $(45/-45)$ increases the torsional frequency. A good compromise can be obtained considering the lamination schemes described by Case 1 and Case 5 that allow the torsional frequency to be increased without

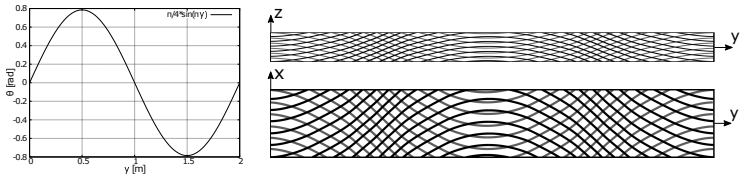

(a) Case 1

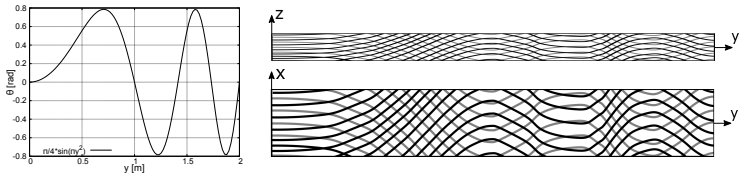

(b) Case 2

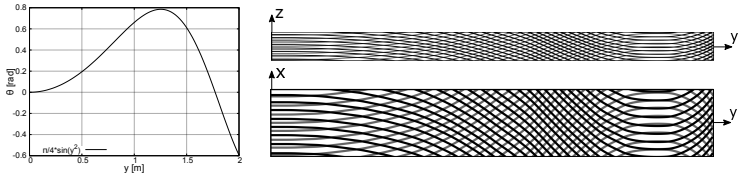

(c) Case 3

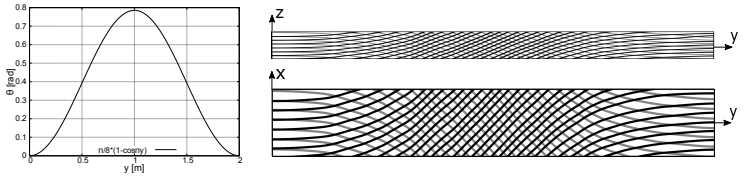

(d) Case 4

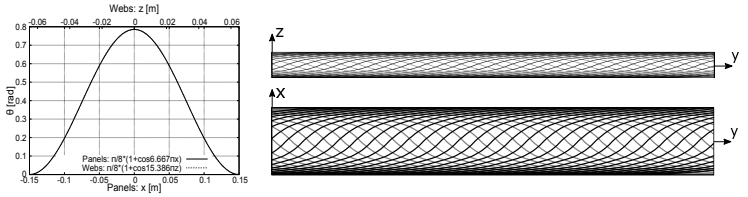

(e) Case 5

Figure 9: Trigonometric laws and fibres-paths for cases one to five.

Case #	Model	$1-B_{xz}$	$1-B_{xy}$	$2-B_{xz}$	$1-T$	$2-B_{xy}$	$3-B_{xz}$	$2-T$	$3-T$
	LE	27.31	52.95	161.27	201.09	304.38	285.11	348.21	507.43
Case 1	TBT	27.66	53.03	176.93	/*	306.24	414.83	/*	/*
	TE4	27.70	53.59	171.84	221.79	309.40	387.13	652.80	1068.25
	LE	28.71	55.55	151.72	206.90	284.71	291.65	358.77	523.76
Case 2	TBT	28.89	55.21	165.25	/*	288.70	437.36	/*	/*
	TE4	29.10	56.10	160.94	226.04	292.09	405.89	661.40	1005.70
	LE	28.81	55.90	151.56	202.91	285.81	293.02	358.76	506.90
Case 3	TBT	29.02	55.52	169.57	/*	291.17	478.25	/*	/*
	TE4	29.23	56.46	162.26	218.44	291.32	430.55	580.33	1004.46
	LE	31.22	60.60	143.23	189.29	267.50	283.58	352.33	506.43
Case 4	TBT	31.87	60.77	164.09	/*	277.99	465.29	/*	/*
	TE4	31.67	61.11	153.79	204.67	272.85	412.42	614.13	999.48
	LE	31.72	60.83	165.63	198.10	312.25	295.11	375.34	526.32
Case 5	TBT	32.20	60.60	186.67	/*	316.01	496.23	/*	/*
	TE4	32.12	61.13	177.88	214.61	316.39	447.87	635.15	1043.97
	LE	31.95	62.23	158.57	194.40	296.69	289.77	363.80	517.44
Case 6	TBT	32.52	62.40	184.25	/*	301.21	490.87	/*	/*
	TE4	32.35	62.62	171.24	208.52	301.21	428.24	617.32	1005.43

/* = modal shape not detected.

Table 5: First eight natural frequency for each VAT configuration.

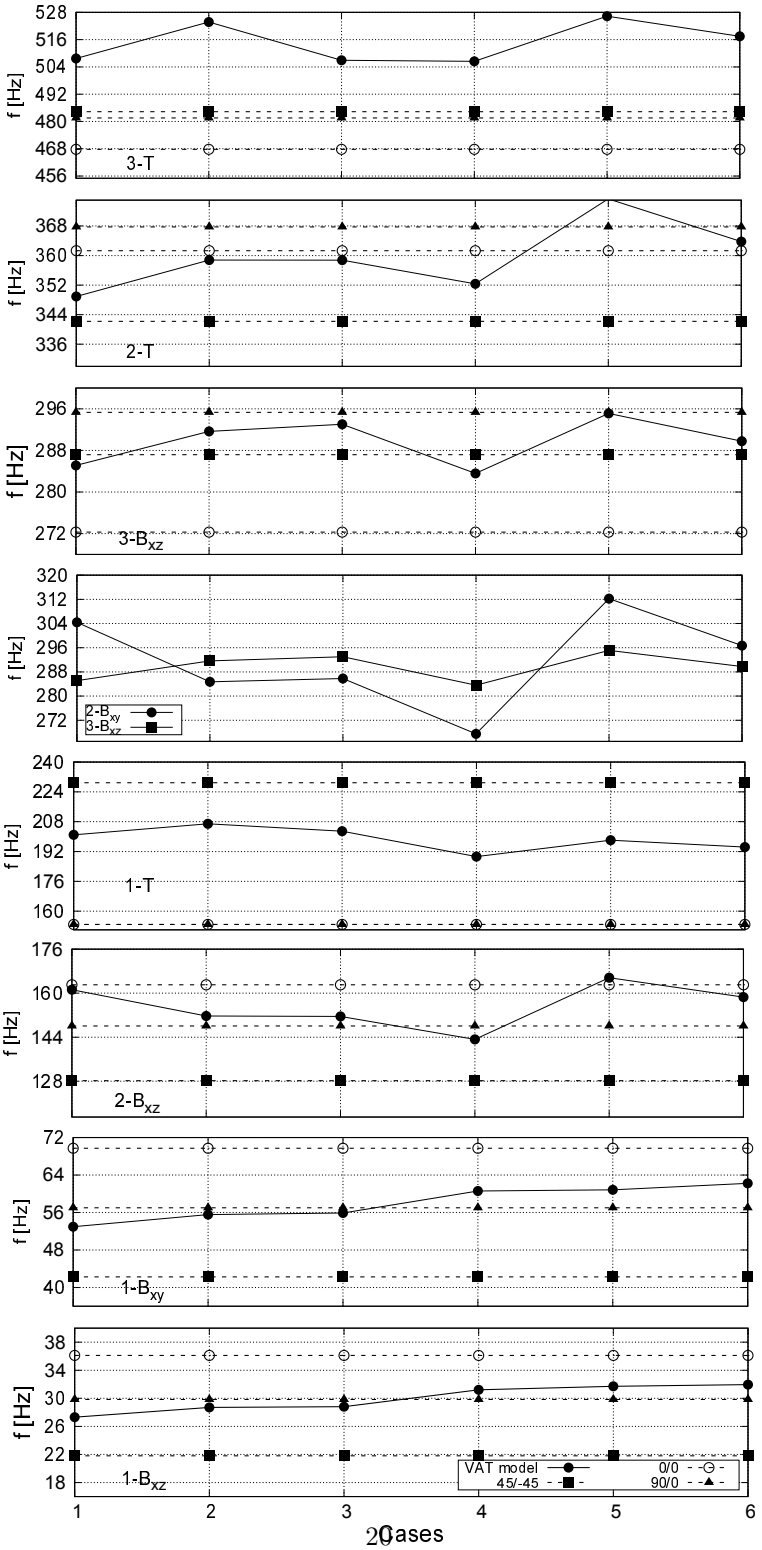

Figure 10: Variation of the frequencies considering different VAT functions compared to the classical laminations.

a drop in the bending performance. Also the frequency related to the second bending modes, see Figures 11b and c, show that VAT Case 1 and 5 allow the bending frequency to be preserved.

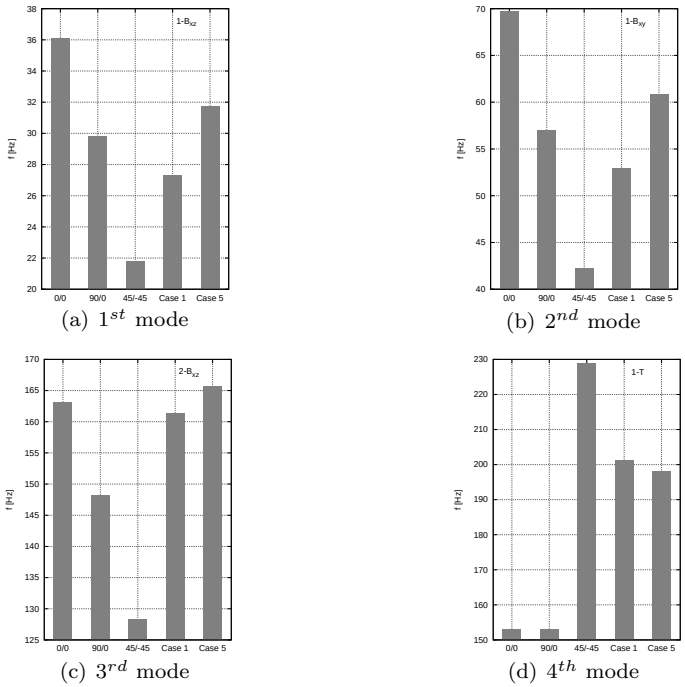

(a) 1^{st} mode (b) 2^{nd} mode

(c) 3^{rd} mode (d) 4^{th} mode

Figure 11: Comparison of the first four frequencies evaluated using classical laminations and VAT cases 1 & 5.

Table 6 highlights the percentage variation of the frequencies. If the unidirectional case is considered as a reference value, the use of a $45°/-45°$ lamination leads to a drop of the 40% of the two bending frequency, while the VAT Case 5 reduces the bending frequencies of the 12%. The torsional frequency shows an increase of the 50% due to the $45°/-45°$ lamination, the use of the VAT models can lead to a comparable increment, about equal to the 30% of the reference value.

3.2. NACA 2415 wing box

This section considers the analysis of a simplified wing structure already studied in the framework of the CUF in the works by Carrera *et al.* [35],

Mode	$0°/0°$	$45°/-45°$	Case 1	Case 5
1^{st} $yz-$ bending	36.11	$21.81^{(-39.60\%)}$	$27.31^{(-24.37\%)}$	$31.72^{(-12.16\%)}$
1^{st} $xy-$ bending	69.70	$42.25^{(-39.38\%)}$	$52.96^{(-24.02\%)}$	$60.83^{(-12.73\%)}$
1^{st} torsional	152.88	$228.28^{(+49.32\%)}$	$200.98^{(+31.46\%)}$	$198.10^{(+29.58\%)}$

Table 6: Variation of the frequencies between classical laminations and VAT cases 1 & 5.

where the free vibration behavior of an isotropic wing, characterized by a NACA profile, has been investigated. Even though a simplified geometry and staking sequence have been considered the model includes the main wing structural components: spars, ribs and skin. The wing profile is shown in figure 12*a* where the internal wing structure can also be appreciated. The wing is composed of two spars obtained by the assembling of the web and four caps. The wing is a full composite structure. The spar web is made of a two-layer laminate as well as the skin and the three transverse equally spaced ribs. The spar caps are unidirectional. The wing length L is equal to 6 m while the chord is equal to 1 m. The spar webs are placed in the first and the third quarter. More details can be found in [35]. Ribs and spar webs are characterized by a $45°/-45°$ stack, while the skin is made of a VAT laminate. As in the previous application, classical laminations have been used for comparison, while the VAT composites have been considered using the previously introduced Case 1 and Case 3. The fibres of the skin have been rotated according to the normal vectors reported in figure 12*a*. A second configuration of the wing box, where the VAT laminates have been used on the skin between the two spars, has also been considered. In this case, the leading and trailing edges have a fixed cross-ply stack. The model is built through a component-wise approach, as shown in Figure 12*b*, using then four nodes beam elements for each component.

The results related to the first five global modes of the structure have been considered, the modal shapes are reported in figure 13. Table 7 reports the frequencies considering classical laminations and the two VAT cases. The results confirm the behaviors due to the classical stacking sequences where, for instance,

310 $45°/-45°$ stack maximizes the torsional frequency. The use of a proper VAT lamination can lead to a compromise in the benefit due to the use of composite materials. For instance, the use of the VAT lamination described by Case 3, ensure the same first bending frequencies of the classical lamination 0/90 but increases the first torsional frequency from 20 to 37 Hz.

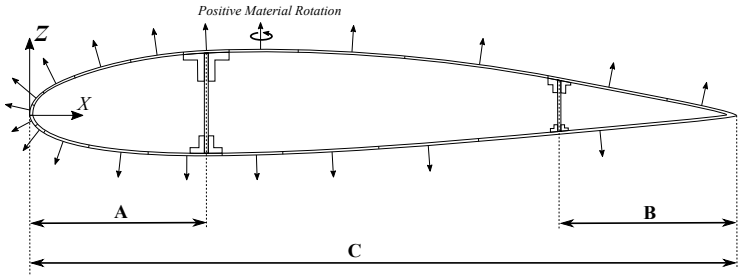

(a) Cross-section of the wing

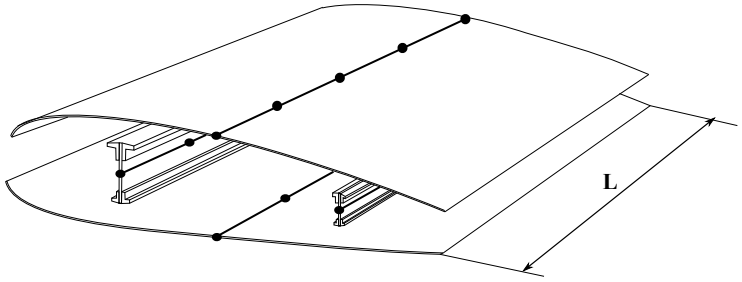

(b) FEM description

Figure 12: NACA 2415 wing profile geometry and its FEM description using the current LE model.

315 The second configuration, in which the leading and trailing edges have been considered with a given cross-ply stack, have also been considered. The use of a VAT lamination only in the region between the spars lead to results comparable to those obtained in the previous case, that is, the wing box plays the most important role in the dynamic of the wing,

320 The effects of the VAT solution on the modal shapes is illustrated in figure 14*a-c*. The fibres-path of Case 3 has an area of unidirectional lamination at the wing tip, that is, a lower torsional stiffness is expected in this wing portion.

Lamination	1^{st} $yz-$Bending	1^{st} $xy-$Bending	2^{nd} $yz-$Bending	1^{st} Torsional	1^{st} Shell-like
			Configuration 1		
$45°/-45°$	4.69	20.46	28.39	59.56	62.87
$0°/0°$	7.83	31.90	36.32	21.10	40.84
$0°/90°$	6.47	27.11	35.91	20.81	73.22
Case 1	5.60	25.43	34.72	41.80	47.82
Case 3	6.56	30.05	30.89	37.02	43.54
			Configuration 2		
Case 3	6.58	30.76	30.94	36.22	43.56

Table 7: Frequencies of the NACA wing box considering classical and VAT laminations

As a consequence, as shown in Figures 14a and b, the torsional deformation is higher at the wing tip. Similarly, Figure 14c represents the shell-like mode that has the most considerable deformations at the root and the tip of the wing when the fibres are placed at $0°$, how said before.

4. Conclusions

The results collected in this work confirm the capability of the presented model to deal with the analysis of VAT composites. The use of a one-dimensional model with a refined kinematic has made it possible to include the curvilinear trajectories of the fibres in the formulation and to predict their effects on the behavior of complex structures. At first, a square thin walled box has been investigated in order to validate the present model comparing the results with those resulting from classical approaches. Different lamination stacks have been introduced by using generic trigonometric functions to describe the lamination angle of the fibres. The results have demonstrated that the use of VAT laminates, can lead to a selective improvement of the dynamic behavior of a structure, e.g., an increment of the torsional frequency can be obtained without a significant reduction in the bending stiffness. The model has been extended to a more complex benchmark: a wing structure with a NACA profile. The results have highlighted what follow:

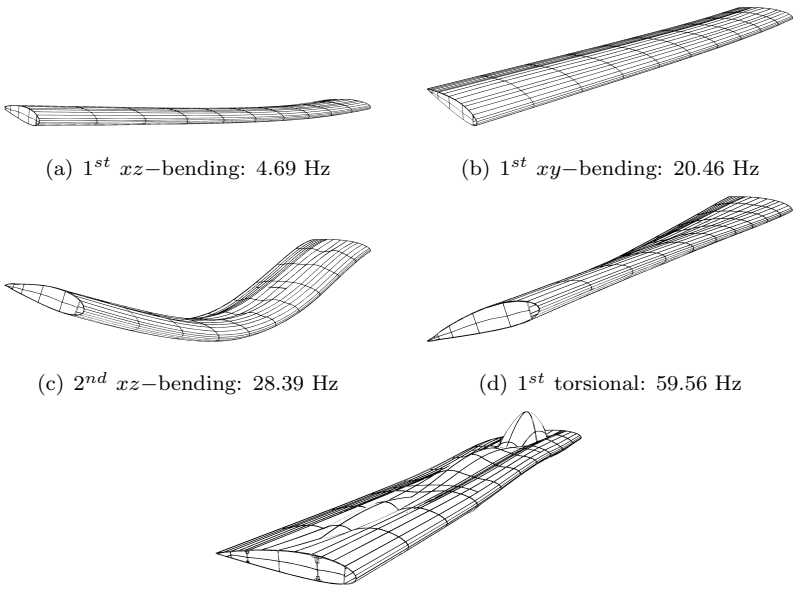

(a) 1^{st} $xz-$bending: 4.69 Hz

(b) 1^{st} $xy-$bending: 20.46 Hz

(c) 2^{nd} $xz-$bending: 28.39 Hz

(d) 1^{st} torsional: 59.56 Hz

(e) 1^{st} shell: 62.87 Hz

Figure 13: Modal Shapes of the NACA wing box: Configuration n.1 with $45°/-45°$ lamination.

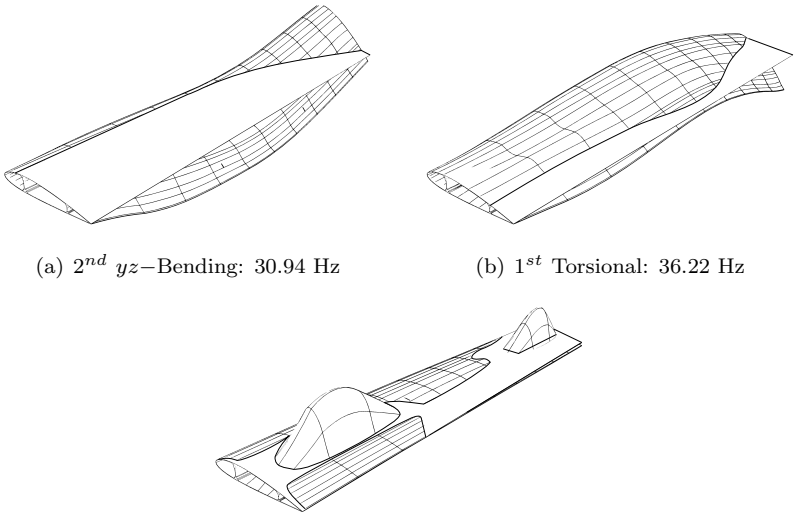

(a) 2^{nd} $yz-$Bending: 30.94 Hz

(b) 1^{st} Torsional: 36.22 Hz

(c) 1^{st} Shell-like: 43.56 Hz

Figure 14: Modal Shapes of the NACA wing box: Configuration n.2 with the VAT Case 3 lamination.

- Refined kinematic one-dimensional models can be used to predict the complex response due to the effect of curvilinear fibres.

- The proper design of the fibres-paths can be used to modify only the desired frequencies, e.g., bending or torsion, without undesired effects on the others.

- The modal shapes can be modified with a proper stiffness distribution.

In conclusion, the present model can be considered a reliable tool for the analysis of VAT structures and could be considered for future applications such as optimization, composite tailoring or aeroelastic analysis. The refined kinematic models adopted in the present work ensure an accurate description of the stress field in the structures, that is, the present approach could be successfully applied to the the analysis of the critical and post-critical response of VAT laminate. Further activities should be performed to include the manufacturing effects.

AppendixA. Fundamental nucleus

The fundamental nucleus, in the case of VAT laminate, can be written in the extended form as follows:

$$
\begin{aligned}
k_{xx} = & \int_V C_{66}F_sF_\tau N_{i,y}N_{j,y}dV + \int_V C_{16}F_sF_{\tau,x}N_iN_{j,y}dV + \int_V C_{16}F_\tau F_{s,x}N_jN_{i,y}dV + \\
& \int_V C_{44}F_{s,z}F_{\tau,z}N_iN_jdV + \int_V C_{11}F_{s,x}F_{\tau,x}N_iN_jdV \\
k_{xy} = & \int_V C_{26}F_sF_\tau N_{i,y}N_{j,y}dV + \int_V C_{66}F_sF_{\tau,x}N_iN_{j,y}dV + \int_V C_{12}F_\tau F_{s,x}N_jN_{i,y}dV + \\
& \int_V C_{45}F_{s,z}F_{\tau,z}N_iN_jdV + \int_V C_{16}F_{s,x}F_{\tau,x}N_iN_jdV \\
k_{xz} = & \int_V C_{45}F_\tau F_{s,z}N_{i,y}N_jdV + \int_V C_{13}F_{s,x}F_{\tau,z}N_iN_jdV + \int_V C_{44}F_{s,z}F_{\tau,x}N_iN_jdV \\
k_{yx} = & \int_V C_{26}F_sF_\tau N_{i,y}N_{j,y}dV + \int_V C_{12}F_sF_{\tau,x}N_iN_{j,y}dV + \int_V C_{66}F_\tau F_{s,x}N_jN_{i,y}dV + \\
& \int_V C_{45}F_{s,z}F_{\tau,z}N_iN_jdV + \int_V C_{16}F_{s,x}F_{\tau,x}N_iN_jdV \\
k_{yy} = & \int_V C_{22}F_sF_\tau N_{i,y}N_{j,y}dV + \int_V C_{26}F_sF_{\tau,x}N_iN_{j,y}dV + \int_V C_{26}F_\tau F_{s,x}N_jN_{i,y}dV + \\
& \int_V C_{55}F_{s,z}F_{\tau,z}N_iN_jdV + \int_V C_{66}F_{s,x}F_{\tau,x}N_iN_jdV \\
k_{yz} = & \int_V C_{23}F_sF_{\tau,z}N_iN_{j,y}dV + \int_V C_{55}F_\tau F_{s,z}N_jN_{i,y}dV + \int_V C_{45}F_{s,z}F_{\tau,x}N_iN_jdV \\
k_{zx} = & \int_V C_{45}F_sF_{\tau,z}N_{j,y}N_idV + \int_V C_{44}F_{s,x}F_{\tau,z}N_jN_idV + \int_V C_{13}F_{s,z}F_{\tau,x}N_jN_idV \\
k_{zy} = & \int_V C_{55}F_sF_{\tau,z}N_iN_{j,y}dV + \int_V C_{23}F_\tau F_{s,z}N_jN_{i,y}dV + \int_V C_{45}F_{s,x}F_{\tau,z}N_iN_jdV \\
k_{zz} = & \int_V C_{55}F_sF_\tau N_{i,y}N_{j,y}dV + \int_V C_{45}F_sF_{\tau,x}N_iN_{j,y}dV + \int_V C_{45}F_\tau F_{s,x}N_jN_{i,y}dV + \\
& \int_V C_{33}F_{s,z}F_{\tau,z}N_iN_jdV + \int_V C_{44}F_{s,x}F_{\tau,x}N_iN_jdV
\end{aligned}
\tag{A.1}
$$

References

[1] M. Hyer, H. Lee, The use of curvilinear fiber format to improve buckling resistance of composite plates with central circular holes, Composite Structures 18 (3) (1991) 239–261. doi:10.1016/0263-8223(91)90035-W.

[2] F. Tornabene, N. Fantuzzi, M. Bacciocchi, A Rayleigh-Ritz approach for postbuckling analysis of variable angle tow composite stiffened panels, Thin-Walled Structures 102 (2015) 222–245. doi:https://dx.doi.org/10.1016/j.tws.2016.01.029.

[3] L. Demasi, G. Biagini, F. Vannucci, E. Santarpia, R. Cavallaro, Equivalent Single Layer, Zig-Zag, and Layer Wise theories for variable angle tow composites based on the Generalized Unified Formulation, Composite Structures 177 (2017) 54–79. doi:https://doi.org/10.1016/j.compstruct.2017.06.033.

[4] P. Ribeiro, H. Akhavan, Non-linear vibrations of variable stiffness composite laminated plates, Composite Structures 94 (8) (2012) 2424–2432. doi:10.1016/j.compstruct.2014.07.007.

[5] P. Ribeiro, Non-linear free periodic vibrations of variable stiffness composite laminated plates, Nonlinear Dynamics 70 (2) (2012) 1535–15482. doi:10.1007/s11071-012-0554-4.

[6] P. Ribeiro, H. Akhavan, A. Teter, J. Warminski, A review on the mechanical behaviour of curvilinear fibre composite laminated panels., Journal of Composite Materials (48) (2014) 2761–2777.

[7] S. Yazdani, P. Ribeiro, A layerwise p-version finite element formulation for free vibration analysis of thick composite laminates with curvilinear fibres, Composite Structures 120 (1) (2015) 531–542. doi:10.1016/j.compstruct.2014.10.030.

[8] S. Yazdani, P. Ribeiro, Geometrically non-linear static analysis of unsymmetric composite plates with curvilinear fibres: p-version layerwise approach, Composite Structures 118 (2015) 74–85. doi:10.1016/j.compstruct.2014.07.007.

[9] M. A. Albazzan, R. Harik, B. F. Tatting, Z. Grdal, Efficient design optimization of nonconventional laminated composites using lamination parameters: A state of the art, Composite Structures 209 (2019) 362 – 374. doi:https://doi.org/10.1016/j.compstruct.2018.10.095.

[10] M. Montemurro, A. Catapano, A general b-spline surfaces theoretical framework for optimisation of variable angle-

tow laminates, Composite Structures 209 (2019) 561 – 578. doi:https://doi.org/10.1016/j.compstruct.2018.10.094.

[11] M. Montemurro, A. Catapano, On the effective integration of manufacturability constraints within the multi-scale methodology for designing variable angle-tow laminates, Composite Structures 161 (2017) 145 – 159. doi:https://doi.org/10.1016/j.compstruct.2016.11.018.

[12] D. M. Peeters, G. G. Lozano, M. M. Abdalla, Effect of steering limit constraints on the performance of variable stiffness laminates, Computers & Structures 196 (2018) 94 – 111. doi:https://doi.org/10.1016/j.compstruc.2017.11.002.

[13] E. Demir, P. Yousefi-Louyeh, M. Yildiz, Design of variable stiffness composite structures using lamination parameters with fiber steering constraint, Composites Part B: Engineering 165 (2019) 733 – 746. doi:https://doi.org/10.1016/j.compositesb.2019.02.004.

[14] W. Zhangming, G. Raju, P. Weaver, Buckling of VAT Plates Using Energy Methods, 53rd AIAA/ASME/ASCE/AHS/ASC Structures, Structural Dynamics and Materials Conference, Structures, Structural Dynamics, and Materials and Co-located Conferences.doi:10.2514/6.2012-1463.

[15] C. Xiaodong, W. Zhangming, N. Guojun, P. Weaver, Buckling analysis of variable angle tow composite plates with a through-the-width or an embedded rectangular delamination., International Journal of Solids and Structures 138 (2018) 166–180. doi:10.1016/j.ijsolstr.2018.01.010.

[16] W. Zhangming, G. Raju, P. Weaver, Postbuckling analysis of variable angle tow composite plates, International Journal of Solids and Structures 50 (10) (2013) 1770–1780. doi:10.1016/j.ijsolstr.2013.02.001.

[17] Z. Wu, P. Weaver, G. Raju, B. Kim, Buckling analysis and optimisation of variable angle tow composite plates, Thin-Walled Structures 60 (2012) 163–172. doi:10.1016/j.tws.2012.07.008.

[18] C. Lopes, P. Camanho, Z. Gürdal, B. Tatting, Progressive failure analysis of tow-placed variable-stiffness composite panels, International Journal of Solids and Structures 44 (25-26) (2007) 8493–8516. doi:10.1016/j.ijsolstr.2007.06.029.

[19] V. Oliveri, A. Milazzo, A Rayleigh-Ritz approach for post-buckling analysis of variable angle tow composite stiffened panels, Computers & Structures 196 (2018) 263–276. doi:https://doi.org/10.1016/j.compstruc.2017.10.009.

[20] O. Stodieck, J. Cooper, P. Weaver, P. Kealy, Improved aeroelastic tailoring using tow-steered composites, Composite Structures 106 (2013) 703–715. doi:10.1016/j.compstruct.2013.07.023.

[21] O. Stodieck, J. Cooper, P. Weaver, Optimisation of Tow-Steered Composite Wing Laminates for Aeroelastic Tailoring, 55th AIAA/ASME/ASCE/AHS/ASC Structures, Structural Dynamics, and Materials Conferencedoi:https://doi.org/10.2514/6.2014-0343.

[22] B. Stanford, C. Jutte, K. Wu, Aeroelastic benefits of tow steering for composite plates., Composite Structures 118 (2014) 416–422.

[23] B. Stanford, C. Jutte, Comparison of curvilinear stiffeners and tow steered composites for aeroelastic tailoring of aircraft wings., Computers & Structures 18 (2017) 48–60. doi:https://doi.org/10.1016/j.compstruc.2017.01.010.

[24] E. Carrera, Theories and finite elements for multilayered plates and shells: a unified compact formulation with numerical assessment and benchmarking., Archives of Computational Methods in Engineering 10 (3) (2003) 215–296.

[25] M. Petrolo, E. Zappino, E. Carrera, Refined free vibration analysis of one-dimensional structures with compact and bridge-like cross-sections., Thin-Walled Struct 56 (2012) 49–61. doi:10.1016/j.tws.2012.03.011.

[26] F. A. Fazzolari, Quasi-3d beam models for the computation of eigenfrequencies of functionally graded beams with arbitrary boundary conditions, Composite Structures 154 (2016) 239 – 255. doi:https://doi.org/10.1016/j.compstruct.2016.06.042.

[27] E. Carrera, M. Petrolo, Refined Beam Elements With Only Displacement Variables and Plate/Shell Capabilities., Meccanica 47 (3) (2012) 537–556.

[28] E. Zappino, A. Viglietti, E. Carrera, Analysis of tapered composite structures using a refined beam theory., Composite Structures 183 (2017) 42–52.

[29] E. Zappino, A. Viglietti, E. Carrera, The analysis of tapered structures using a component-wise approach based on refined one-dimensional models., Aerospace Science and Technology 65 (2017) 141–156.

[30] E. Viglietti, E. Zappino, E. Carrera, Analysis VAT composites structures using variable kinematic models, Composites Part B: Engineering.In Press.

[31] E. Zappino, E. Carrera, Multidimensional model for the stress analysis of reinforced shell structures, AIAA Journal 56 (4) (2018) 1647–1661, doi: 10.2514/1.J056384.

[32] E. Carrera, M. Cinefra, M. Petrolo, E. Zappino, Finite Element Analysis of Structures Through Unified Formulation, John Wiley & Sons, 2014.

[33] J. Reddy, Mechanics of laminated composite plates and shells. Theory and Analysis, 2nd Edition, CRC Press, 2004.

[34] E. Carrera, M. Petrolo, E. Zappino, Performance of cuf approach to analyze the structural behaviour of slender bodies, Journal of Structural Engineering 138 (2) (2012) 285–297, doi: 10.1061/(ASCE)ST.1943-541X.0000402.

[35] E. Carrera, A. Pagani, M. Petrolo, Component-wise method applied to vibration of wing structures., Journal of Applied Mechanics 80 (4) (2013) Paper 041012. doi:10.1115/1.4007849.